Computer simulation study on the concentration distribution of spherical colloids within confined spaces of well-defined pores

Myung-Suk Chun

Polymer Division, Korea Institute of Science and Technology, P.O. Box 131, Cheongryang, Seoul 130-650, Korea
mschun@kistmail.kist.re.kr

(Received: January 14, 1999; revised: March 26, 1999)

SUMMARY: Aside from the virial expansion and density functional methods, theoretical results on the concentration partitioning behavior for charged colloids within cylindrical pores have not been presented so far. With the increase of relative solute size as well as solute concentration, however, the approximate analytic methods have proven to be unreliable. A suitable Monte Carlo simulation, which is proved as a rigorous technique for concentrated colloids, has been applied in the present study. The concentration profiles within the pore representing the effects of solute concentration as well as solution ionic strength are obtained via a stochastic process, from which the partition coefficient is estimated. Previously developed analyses on the linearized Poisson-Boltzmann (P-B) equation are employed for the estimation of long-range electrostatic interaction. Both the singularity method and the analytical solution with series representation properly determine respective interaction energies between pairs of solute particles and between the solute particle and the pore wall. The effect of solute-solute and solute-wall interactions associated with repulsive energy is presented on the partitioning of colloids. Simulation results show that the partition coefficient is evidently enhanced when no particle-wall interaction exists. Hindered diffusion can be predicted by the simplifying assumption of the centerline approximation analogy, where a dependence on the solute concentration becomes greater as the solution ionic strength decreases.

Introduction

The transport of colloids through pores of molecular dimensions is slower than in bulk solution. The hindered transport in confined spaces of pores is an ingredient of both natural and engineered mass transfer[1–3]. The simplest and usual approach in hydrodynamic models has been to identically represent the porous medium as an assemblage of long, straight, cylindrical pores. This geometry is a literal descriptor of the circular pores present in track-etched polycarbonate membranes. The solute and solvent fluxes in hydrodynamic models are evaluated by solving the equations of motion for a spherical solute in a well-defined pore.

The desired local flux equation is obtained from the mean macroscopic quantity regarding the flux averaged over the cylindrical pore cross section, $\langle J_s \rangle$

$$\langle J_s \rangle = Q_c \langle v \rangle \langle C \rangle - Q_d D_\infty \frac{\mathrm{d}\langle C \rangle}{\mathrm{d}z} \qquad (1)$$

Here Q_c and Q_d are the convective and diffusive hindrance factors, C is the local solute concentration, $\langle v \rangle$ is the mean fluid velocity, and D_∞ corresponds to the free solution diffusion coefficient at infinite dilution. Many colloids and macromolecules such as latex particles and proteins carry charges in aqueous solution, as do the solid walls of the membrane pore. In a polyelectrolyte system, both the steric and the electrostatic interactions determine the spatial distribution of the particle in the pore. This distribution is usually expressed in terms of the partition coefficient K, defined as the ratio of mean pore-to-bulk concentration at equilibrium:

$$K = \int_0^{1-\lambda} C(\beta)\beta \mathrm{d}\beta \Big/ \int_0^1 C(\beta)\beta \mathrm{d}\beta \qquad (2)$$

where λ and β are the solute radius and radial coordinate, respectively, both normalized by the pore radius. It is obvious that efforts to elucidate the membrane transport properties have been almost confined to the case of infinitely dilute solute concentration. For dilute solutions, the concentration profile $C(\beta)$ of Eq. (2) can be represented by a Boltzmann distribution involving the long-range interaction energy between the solute particle and the pore wall. In general, however, the solute concentrations in the real situation of colloidal dispersion can not be considered dilute. For non-dilute solute concentrations, modeling hindered transport behavior is truly more difficult, in which the effects of particle-particle interactions on $C(\beta)$ must be included.

In the early 1980s, Glandt[4] developed a virial expansion method for the concentration partitioning in powers of the bulk concentration, and he calculated the second and third virial coefficients for hard-sphere solutes in regular geometric pores. Whereas only steric interactions were considered in his work, Anderson and Brannon[5]

  1022-1344/99/0509–0418$17.50+.50/0

addressed some results for concentration profiles including the electrostatic interactions. Subsequently, Mitchell and Deen[6] analyzed the effects of electrostatic interaction on the concentration partitioning of charged colloids, by employing the virial expansion method in the context of cylindrical pores. With increasing the solute concentration, partition coefficients are found to increase, however, the solute rejection from the pore is decreased. The partitioning behavior of charged colloids in the dilute limit of solute concentration was analyzed in detail by Smith and Deen [7]. Davidson et al.[8] investigated the partitioning problem of flexible macromolecules by using a Monte Carlo scheme taking into account the random coil conformation, in which the solute concentration was sufficiently dilute, too. By adopting linear density function theory, Post[9] calculated the effect of solute concentration at concentrations where the virial expansions are not expected to be accurate. Readers interested in the basic mechanism of the transport process may be referred to Deen's review article[3], where the hydrodynamic continuum theory for the convective and diffusive transports of suspensions of neutral, rigid spheres within cylindrical pores was conducted. Later, Lin and Deen[10] examined the influence of electrostatic interactions on the diffusion of linear polymers through track-etched polycarbonate membranes with narrow pores, where the hindered diffusion decreases at low salt concentrations.

However, the perturbed approximations such as virial expansion or density functional scheme have been widely known to be unsuitable methods to predict the concentration partitioning for larger relative solute size as well as higher solute concentration. A stochastic Monte Carlo method has been found to be useful indeed to overcome this kind of problem. MacElroy and Suh[11] have reported a grand canonical Monte Carlo (GCMC) simulation trial for hard spheres in the cylindrical pore, from which the limitation of Glandt's work for higher bulk concentrations was explicitly revealed. The GCMC simulation has been also applied to the partitioning within disordered porous solids[12]. The results of the low-dimensional approach for the partitioning within adsorbing narrow pores demonstrated a correspondence to the GCMC results[13]. Since Panagiotopoulos[14] firstly proposed the Gibbs ensemble Monte Carlo (GEMC) method, this approach has been mainly used with considerable success to study the problems of phase equilibria[15–18]. Recently, Chun and Phillips[19] studied the electrostatic partitioning of spherical colloids within the simple geometry of slit-like pores. According to their results, the GEMC technique has been proved to be a rigorous scheme to examine concentrated colloids for the whole range of relative solute size involving the interaction energy.

To be sure, it is important to establish a framework to predict concentration partitioning and hindered diffusion of colloids in terms of the geometric structure such as solute to pore ratio, the physicochemical parameters such as ionic strength, surface potential (or charge density), and the solute concentration. In this study, the influence of electrostatic interactions on the concentration distribution of concentrated colloidal suspensions is examined by using the GEMC simulation, where the solute concentrations range up to 20 vol.-%. This distribution is then used to estimate the hindered diffusion by considering the transport of spherical solutes through the cylindrical pores. Simulation results of the concentration profile in the pore are compared with the results calculated by performing virial expansions.

Stochastic Monte Carlo simulations

The principle of Gibbs ensemble Monte Carlo techniques

It has been proved that the Monte Carlo method is characterized by the greatest precision, accuracy, and subtlety, in modeling probabilistic processes with the statistical mechanical principle. The basic concept of the Monte Carlo scheme can be found in the relevant literature (cf., e.g., refs.[20] and [21]). As noted above, the GEMC method is available to apply favorably to the problem of partitioning of concentrated solutes within bounded spaces. Compared to the GCMC method, this one is particularly suited when long-range interaction energies are considered. The Gibbs ensemble consists of the elements of canonical (*NVT*), isobaric-isothermal (*NPT*), and grand canonical (μVT) ensembles, from which the GEMC method allows one to simulate the coexisting subsystems consisting of a pore and a bulk region. It was mentioned in the previous work[19] that exchanges of the volume between the two regions of the solid pore and the bulk do not need to be included. As a result, both the particle displacement and the interchange moves are performed in the computational cycle of the present GEMC simulations.

Periodic unit cells are constructed with cylindrical and Cartesian coordinates for the pore and the bulk region, respectively. The cylindrical pore is assumed to extend to infinite in the axial (i.e., y) direction; as a consequence, periodic boundary conditions are imposed for the y-direction. The bulk has a cubic unit cell, and the periodic boundary conditions are readily imposed for all directions. The solute volume fraction and the number of solutes determine the dimension of each unit cell. States in the canonical ensemble of the *NVT* Metropolis process occur with a probability proportional to $\exp(-E^{\alpha}/(kT))$ for an arbitrary subsystem α. Here, E^{α} means the interaction energy in subsystem α caused by the random displacement, and kT is the Boltzmann thermal energy. The new configurations are generated with a probability p_D given by

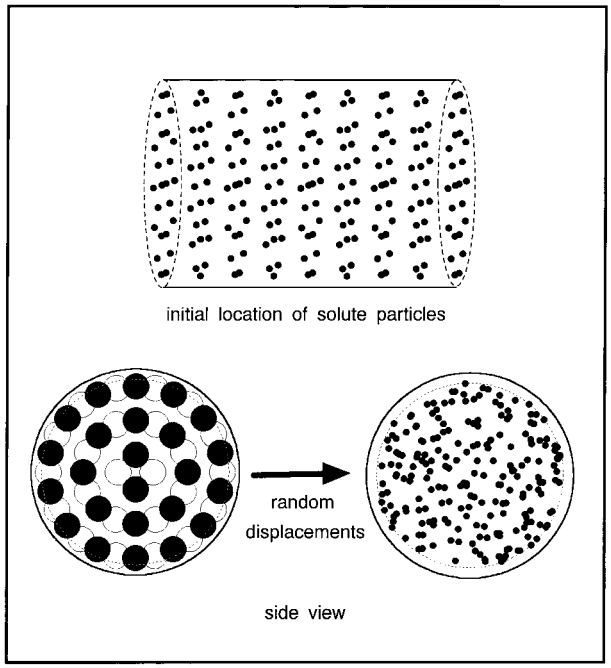

Fig. 1. Illustration of the initial and final positions of the solutes in a pore by performing random displacements of GEMC simulation for λ = 0.1 and solute concentration of 10 vol.-%. The small-sized spheres represent the center-of-mass positions of each solute. The left side view displaying a staggered configuration corresponds to the real size

$$p_D = \min\left[1, \exp\left(-\Delta E^{\alpha}/(kT)\right)\right] \tag{3}$$

where ΔE means $E_{\text{new}} - E_{\text{old}}$. In the μVT process, the probability of the grand canonical ensemble governing the particle transfer from subsystem α to subsystem β is provided as

$$p_T = \min\left[1, \exp\left\{-\left(\frac{\Delta E^{\alpha} + \Delta E^{\beta}}{kT}\right) + \ln\left(\frac{N^{\alpha} V^{\beta}}{(N^{\beta}+1)V^{\alpha}}\right)\right\}\right] \tag{4}$$

Fig. 1 illustrates a physical situation for the case of purely steric interaction, describing the change of particle configurations by random displacements in the *NVT* process in the pore region. In the GCMC, a consistent computation breaks down with increasing colloid concentration due to the nature of the method, in which it becomes difficult to insert solute particles. In addition, the whole annihilation of particles in the specific region (frequently, a simulation box in the narrow pore) is maintained, when the μVT process of particle transfer is taken alone. Subsequent configurational changes by particle displacements remove this kind of abnormal establishment, explaining the role of the *NVT* process in the GEMC.

Computational considerations

The computational procedure is similar to the earlier idea pertaining to the slit-like pore[19]. As the initial locations, particles are arranged in face-centered unit lattices in both a bulk and a pore region. Usually, 500 to 1300 solute particles are introduced. The solute radius is held constant at 20 nm, and the pore radius is varied to achieve different values of the ratio λ. The bulk solute volume fraction is given by $(4/3)\pi a^3 N_b/V_b$, where N_b/V_b equals to the solute number density in the bulk.

The test for overlap in random moves of particles is performed with the square-well mode, where no interaction occurs between the particles until contact or very close approach between the surfaces occurs and then the interaction potential becomes infinite. The relevant adjustment parameters, which account for the step sizes of the random displacements and the number of particles transferred successfully, were chosen with a value similar to the previous work. Random numbers between 0 and 1 were necessarily generated in all computations so as to determine whether or not to accept a new configuration. The respective moves are accepted if the random number is less than the probabilities computed from Eqs. (3) and (4). In general, about $1-3\times10^4$ configurations are required to reach equilibrium, and discarding the non-equilibrium configurations. Thereafter, the averages are accumulated over additional $3-20\times10^4$ production configurations. As a simulation proceeds, the partition coefficient calculated by using smaller numbers of particles fluctuates somewhat more than that for systems with larger numbers. For the radial density profile the pore cross-section is divided into equal radial increments of shell width, and the number density in each radial increment is calculated. The overall algorithm coded by FORTRAN is presented in Fig. 2. Both a Hewlett-Packard 9000 715/100 workstation and a CRAY-C90 supercomputer have been used to carry out the simulations.

The simulation results for the partition coefficient of uncharged systems are addressed in Fig. 3, where the infinite dilution partition is equivalent to $K = (1-\lambda)^2$. The partition coefficient K, plotted as a function of λ, affects the variation of the membrane transport coefficient with solute concentration. For comparison, earlier results predicted from virial expansions[4] as well as the GCMC simulations[11] are plotted here. It can be seen that, for λ less than 0.2, present GEMC results are nearly identical to the virial expansion method for values of bulk solute concentration up to 20 vol.-%. At bulk concentrations of 10 and 20 vol.-%, the K curve shows a rising feature for strongly confined spaces with values of λ greater than 0.5. Note that the previous results based on the virial expansion method can not predict this interesting rise. As an appropriate formalism regarding this fact, the low-dimensional approach was proposed earlier[13]. Likewise

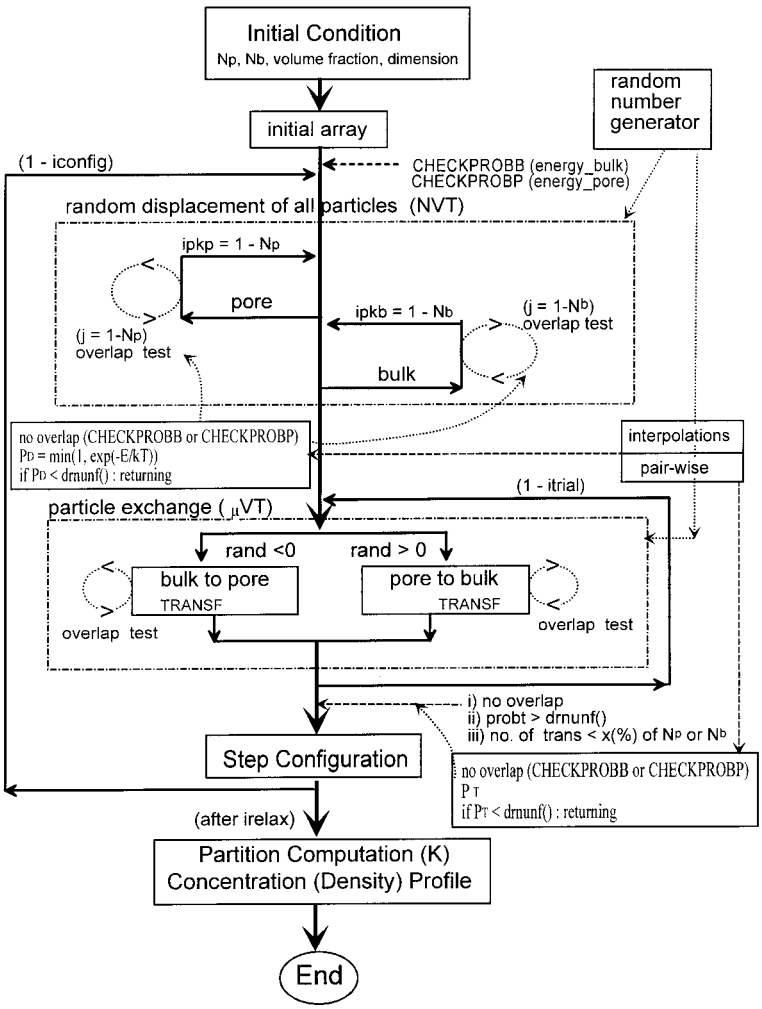

Fig. 2. GEMC simulation scheme

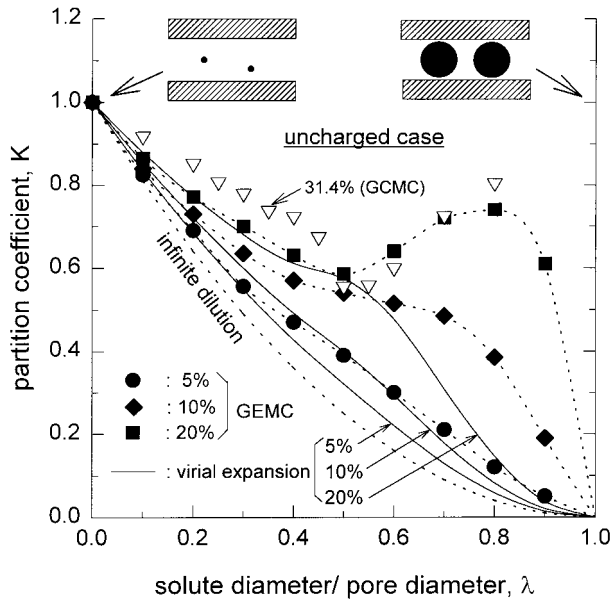

Fig. 3. Comparison of the prediction of a purely steric partition coefficient K for various solute concentrations between the present GEMC, GCMC[11] and virial expansion methods[4]

in a recent analysis of slit pore systems[19], the development of close-packed hard rods of solute within the narrow pore hypothetically accounts for this behavior.

Solute concentration profiles within the pore

Virial expansion

We implement a computation of the partition coefficient by using a virial expansion to compare with the GEMC results, as treated in the previous work. With the solute concentration in the bulk C_b, the solute concentration profile $C(h)$ is expressed by

$$C(h) = C_b \mathrm{e}^{-E(h)/(kT)}\left(1 + C_b Y_1(h) + \ldots\right) \qquad (5)$$

where

$$Y_1(h) = \int \left(\mathrm{e}^{-E(h)/(kT)} - 1\right) f(\boldsymbol{r}, \boldsymbol{r}_1)\mathrm{d}\boldsymbol{r}_1 = \int \left(\mathrm{e}^{-E(h)/(kT)} - 1\right)\left(\mathrm{e}^{-E(\boldsymbol{r},\boldsymbol{r}_1)/(kT)} - 1\right)\mathrm{d}\boldsymbol{r}_1 \qquad (6)$$

In the above equation, one sphere is at position $\boldsymbol{r}$, a separation distance h from the pore wall, and a second sphere is at position $\boldsymbol{r}_1$. The integral is over all space within the cylindrical pore, and the Mayer function $f(\boldsymbol{r}, \boldsymbol{r}_1)$ depends on the solute-solute interaction. For the charged case, the energy profiles should be provided, for which the relevant analogies are described in the following section. Y_1 is defined in terms of configuration-space integrals that involve both solute-wall and solute-solute interactions.

Uncharged case

The concentration profile of solute particles can be identified from the monitoring of the density profile. Fig. 4 illustrates the radial density profiles of a cylindrical pore for which $\lambda = 0.3$. The stochastic fact that the solute density is relatively high near the inert pore wall is typical in equilibrium partitioning of the uncharged case. When the solute concentration C_b is increased to 20% from 5%, the density profile becomes more oscillating. By employing an effective collection and the averaging scheme for every GEMC run, the fluctuations in concentration profiles are considerably reduced compared to the previous study. The density profiles from the GEMC are compared with corresponding predictions from the virial expansions, and agree well entirely at a solute concentration of 5%. The discrepancy between the two methods is shown at 20%, which is related to the results of the partition coefficient presented in Fig. 3.

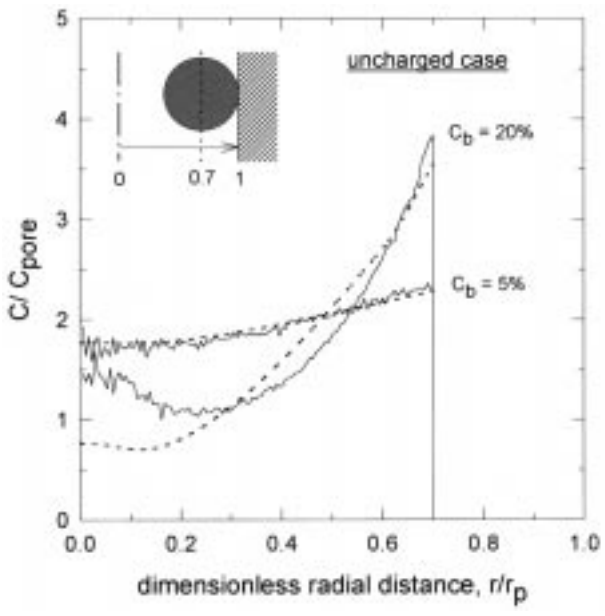

Fig. 4. Density profiles of uncharged solutes in a cylindrical pore for $\lambda = 0.3$ and solute concentrations of 5 and 20 vol.-%. Dashed curves correspond to virial expansion results

Charged case

When the pore wall and the solutes are charged, electrostatic interactions contribute to the energy E in Eqs. (3) and (4). Solving the complete Poisson-Boltzmann (P-B) equation remains a great challenge because of the nonlinear nature of the equation, which governs the electrostatic potential of the system. It is indeed common to adopt a linearized P-B equation, given by

$$\nabla^2 \psi = (\kappa a)^2 \psi \tag{7}$$

where the electrostatic potential ψ is normalized by a characteristic surface potential, and the inverse Debye length κ is made dimensionless by the solute radius a[22]. Two kinds of boundary conditions, which correspond to the constant charge and constant potential conditions, can be commonly used in obtaining solutions for Eq. (7). In this study, we assume that the solute and pore surfaces S have a constant surface-charge density σ, leading to the constant charge boundary condition

$$\boldsymbol{n} \cdot \nabla \psi = \sigma \text{ on } S \tag{8}$$

where $\boldsymbol{n}$ denotes a unit normal vector. Except for only surface separations so small as to be rendered highly improbable, the linearized P-B equation with constant charge boundary conditions provides a good accuracy. From the singular solution of Eq. (8) for a point charge at the origin, each of the dimensionless surface charge densities of the wall and the solute are expressed as

$$\sigma_w = \psi_{s,w}(\kappa a) \text{ (for wall)} \tag{9}$$

$$\sigma_p = \psi_{p,w}(\kappa a + 1) \text{ (for solute)} \tag{10}$$

In the Debye-Hückel limit of Eq. (7), both the pore wall and solutes, when they are isolated and not interacting with each other, have fixed surface potentials kT/e = 25.69 mV, where e is the elementary electrostatic charge.

The electrostatic potential between pairs of spherical solutes is determined by using a singularity method, in which accurate solution of the P-B equation is successfully provided[19, 23]. Here, the singularity method uses a pointwise distribution of the Green function as the solution and determines the strength of each singularity by satisfying the boundary conditions at each point. Accounting for the spherical coordinate with each component of unit vector $\boldsymbol{e}_r$, $\boldsymbol{e}_\theta$, and $\boldsymbol{e}_\varphi$ calculates the force on an arbitrary charged sphere interacting with other charged spheres. Then, the electrostatic interaction energy profile with separation distance h can be obtained by integrating the force acting on the sphere as follows

$$E_{ss}(h) \equiv \int_{-\infty}^{h} F_z \, \mathrm{d}z = \int_{-\infty}^{h} \left[\boldsymbol{e}_z \cdot \int_S \boldsymbol{T} \cdot \boldsymbol{n} \, \mathrm{d}S \right] \mathrm{d}z \tag{11}$$

$$= \int_S \left[\cos(\theta)\boldsymbol{e}_r \cdot \boldsymbol{T} \cdot \boldsymbol{e}_r - \sin(\theta)\boldsymbol{e}_\theta \cdot \boldsymbol{T} \cdot \boldsymbol{e}_r\right] \mathrm{d}S$$

$$= \int_S \left[\cos(\theta)T_{rr} - \sin(\theta)T_{\theta r}\right] r^2 \sin(\theta)\mathrm{d}\theta\mathrm{d}\varphi$$

In Eq. (11), the Maxwell stress tensor $\boldsymbol{T}$ determined from electric field vector $\boldsymbol{E}$ (= $-\nabla\psi$) and osmotic pressure Π is given by

$$\boldsymbol{T} = (\Pi + \varepsilon \boldsymbol{E} \cdot \boldsymbol{E}/2)\boldsymbol{I} - \varepsilon \boldsymbol{E} \cdot \boldsymbol{E} \qquad (12)$$

where ε is the dielectric constant, and $\boldsymbol{I}$ is identity tensor.

The next issue that we should examine is the electrostatic interaction energy between the wall of a cylindrical pore and the spherical solute. When the solid wall has a planar interface found in the slit pore, the combination of image singularity and actual singularity is guaranteed faithfully. However, the generalization of this method to the curved wall of a cylindrical pore is not valid any more. Smith and Deen[7] presented analytical expressions for the electrostatic energy of a spherical colloid in a cylindrical pore. They obtained series representations of the electrostatic potential within the pore and membrane space by solution of the linearized P-B equation. In principle, a tractable relation for the change in interaction energy between the sphere and pore wall is expressed as

$$E_{sw}(h) = E_{com} - E_{w,iso} - E_{s,iso} \qquad (13)$$

where the subscripts *s,iso*, *w,iso*, and *com* refer to the isolated sphere, isolated pore wall, and combined sphere-wall system, respectively. Note that the energy for a system at constant charge density is possibly evaluated by integrating the surface potential over the charged surface *S*

$$E = \frac{\sigma}{2}\int_S \psi_s(\sigma)\mathrm{d}S \qquad (14)$$

The total energies of both regions after the particle displacements and interchanges are evaluated by using a pairwise additive principle with respect to the wall-particle and particle-particle interactions. The reliability of this principle for such interactions can be acceptable as discussed later. Basically, we assume that the interaction energy among *N* particles is a sum of isolated pair interactions *E*. The expression for the bulk region is given by

$$E_{total}^{bulk} \equiv E_{s-s}^{bulk} = \sum_{j=1+1}^{N}\sum_{i=1}^{N} E(h_{ij}) \qquad (15)$$

and for the region of a cylindrical pore

$$E_{total}^{pore} \equiv E_{s-s}^{pore} + E_{s-w}^{pore} = \sum_{j=1+1}^{N}\sum_{i=1}^{N} E(h_{ij}) + \sum_{i=1}^{N} E(h_{iw}) \qquad (16)$$

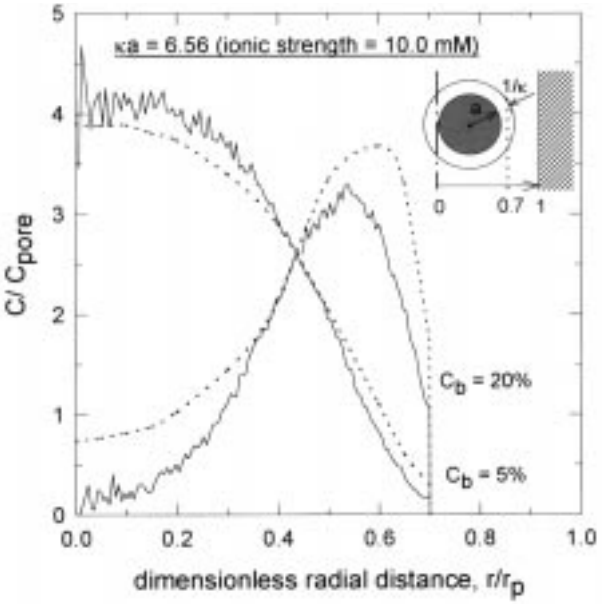

Fig. 5. Density profiles of charged solutes in a cylindrical pore for κa = 6.56 (i.e., ionic strength = 10 mmol/L), λ = 0.3 and solute concentrations of 5 and 20 vol.-%. Dotted curves correspond to virial expansion results

where h_{ij} is the distance between the centers of particles *i* and *j*, $h_{ij} = |\boldsymbol{h}_i - \boldsymbol{h}_j|$. The interpolation with polynomials described in the previous work is adopted again so as to determine instantaneously the interaction energy at arbitrary particle-particle and particle-wall separation distances. Fig. 5 shows radial density profiles for charged solutes with bulk concentrations of 5 and 20% at ionic strength of 10 mmol/L in a charged pore for which λ = 0.3. For aqueous solutions of monovalent electrolytes at 25 °C, the inverse Debye length κ(in nm^{-1}) is given by 3.278 ×[ionic strength (in mol/L)]$^{1/2}$. Compared to the uncharged case, the repulsive electrostatic interactions evidently decrease the concentration near the pore wall. As the solute concentration increases, however, the effect of solute-solute interaction is to shift a region of enhanced concentration toward the pore wall. Profiles obtained by the virial expansion method are also provided for comparison. The two sets of results are likely in agreement at the lower solute concentration of 5%, but obvious disagreement can be seen at 20%. Further, although not provided here, it is clear that this disagreement is developed with increasing of λ.

Discussion

Concentration partitioning

The presence of electrostatic interactions affects the partitioning in cylindrical pores. Based on the previous verification[23], the application of pairwise additivity for the sphere-sphere interaction is quite reliable. This is

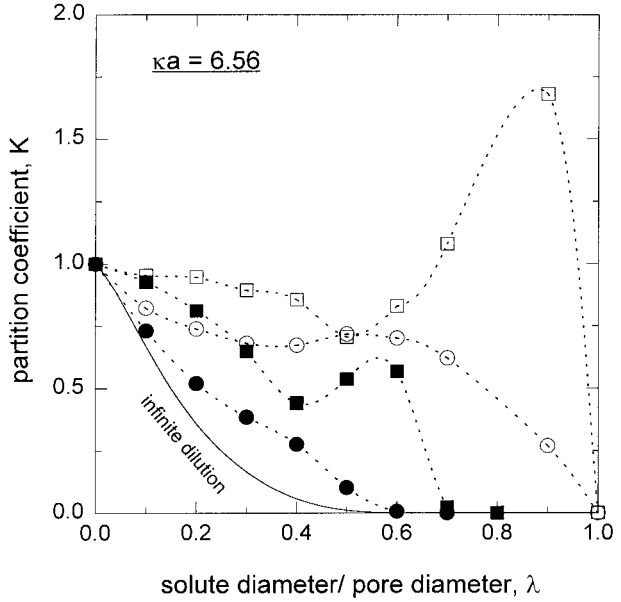

Fig. 6. Comparison of partition coefficients for the case of uncharged wall-charged solutes and for the case of charged wall-charged solutes with solution ionic strength of 10 mmol/L; ●: charged wall-charged solute with 5 vol.-% solute concentration, ○: uncharged wall-charged solute with 5 vol.-% solute concentration, ■: charged wall-charged solute with 20 vol.-% solute concentration, □: uncharged wall-charged solute with 20 vol.-% solute concentration

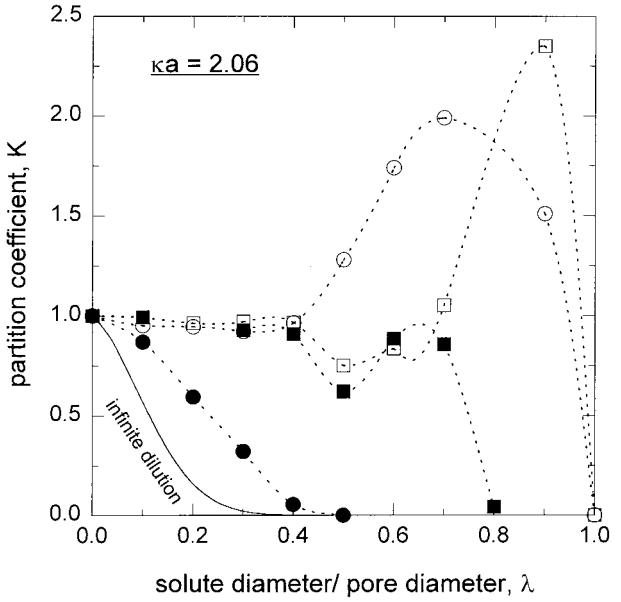

Fig. 7. Comparison of partition coefficients for the case of uncharged wall-charged solutes and for the case of charged wall-charged solutes with solution ionic strength of 1 mmol/L; ●: charged wall-charged solute with 5 vol.-% solute concentration, ○: uncharged wall-charged solute with 5 vol.-% solute concentration, ■: charged wall-charged solute with 20 vol.-% solute concentration, □: uncharged wall-charged solute with 20 vol.-% solute concentration

because, in the present study, both the values of κa and the nearest distance between two spheres evaluated from solute volume fraction are in reliable ranges. Even though exact verification is not available, the application of pairwise additivity for the curved wall-sphere interaction is also reasonable. The sphere-sphere interaction is dominant for lower λ so that the error order resulting from sphere-wall interaction is sufficiently low. Further, no discrepancy is encountered for higher λ, since the partitioning itself becomes really zero. Possible errors may occur, when solutes with higher concentration are simulated in the intermediate λ region. Nevertheless, the pairwise additivity itself can not produce a wide discrepancy, when the particle radius is larger than the Debye length (i.e., $\kappa a > 1$).

The influence of solute concentration is investigated by comparing the partition coefficients obtained by particle-particle interaction alone with those obtained by particle-particle and particle-wall interactions. As shown in Fig. 6 and 7, the partition coefficient is enhanced when the particle-wall interaction does not exist. In this case, the double layer interaction between pore wall and solute particles is not influenced, hence, the pore region will be occupied with a sufficiently large number of particles. Once λ is over about 0.5 for the case of particle-particle interaction alone, the partition coefficient becomes larger than one. When the Debye length increases, corresponding to κa = 2.06, the enhanced partitioning is more considerable as shown in Fig. 7. It is common that the partitioning enhancement is increased as the pore becomes narrower. The enhanced behavior of the partition coefficient for the system of uncharged wall and charged solutes seems to result in a situation that a physical adsorption of solutes within the pores is favorably experienced.

Hindered diffusion coefficient

The diffusion coefficient for colloids in the membrane pore (D^p) tends to be lower than that in an unbounded solution (D_∞). Neutrally buoyant rigid solutes suspended in the solvent are treated as a continuous Newtonian fluid, in which the familiar Stokes-Einstein equation is easily applied as

$$D_\infty = \frac{\kappa T}{6\pi\eta a} \tag{17}$$

where the solvent viscosity is given by η, and ($6\pi\eta a$) corresponds to the molecular friction coefficient. The ratio of diffusion is characterized by the hindered diffusion coefficient H, defined as

$$H \equiv \frac{D^p}{D_\infty} \tag{18}$$

This equals to the product of partition coefficient K and diffusive hindrance factor Q_d. The diffusive hindrance

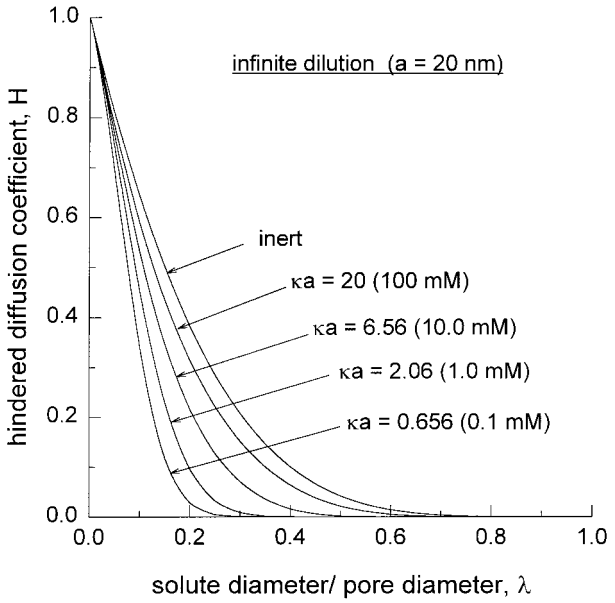

Fig. 8. Hindered diffusion coefficient H at infinite dilution as a function of λ for several ionic strengths

factor can be obtained from the hydrodynamic coefficient Q^{-1}, which is related to the enhanced drag incorporating the effects of pore wall. Q^{-1} should be basically determined by computing the drag on a charged sphere translating parallel to the tube axis, however, relevant results for the charged case with wide range of λ are not currently available. Since implementation of the hindered transport theory has been handicapped to some extent by a lack of complete hydrodynamic information, current development leads to use of the centerline approximation. While this assumption is incomplete in a sense of exactness, it should lead at least qualitatively, and in some cases quantitatively, to accurate estimates. Then, Eq. (18) becomes to

$$H = KQ^{-1} = K\left(\frac{6\pi}{K_t}\right) \tag{19}$$

where the function K_t given in the literature is expressed as expansions in λ with the closely fitting coefficients[24]. Note that this expression has increased accuracy for larger values of λ, and accuracy within 10% for all relative pore sizes is available.

In the dilute limit, the solute-solute interactions are negligible. The repulsion between the solute and the pore wall having surface charges of the same sign leads to a sharp decrease in the hindered diffusion coefficient H as shown in Fig. 8. Ionic strengths range from 0.1 to 100 mmol/L, and H approaches eventually the inert hard-sphere results, with the increase of κa. The hindered diffusion coefficient H for the uncharged case is estimated as shown in Fig. 9a. H is nearly zero with λ above about 0.8, which means that particle diffusion does not occur

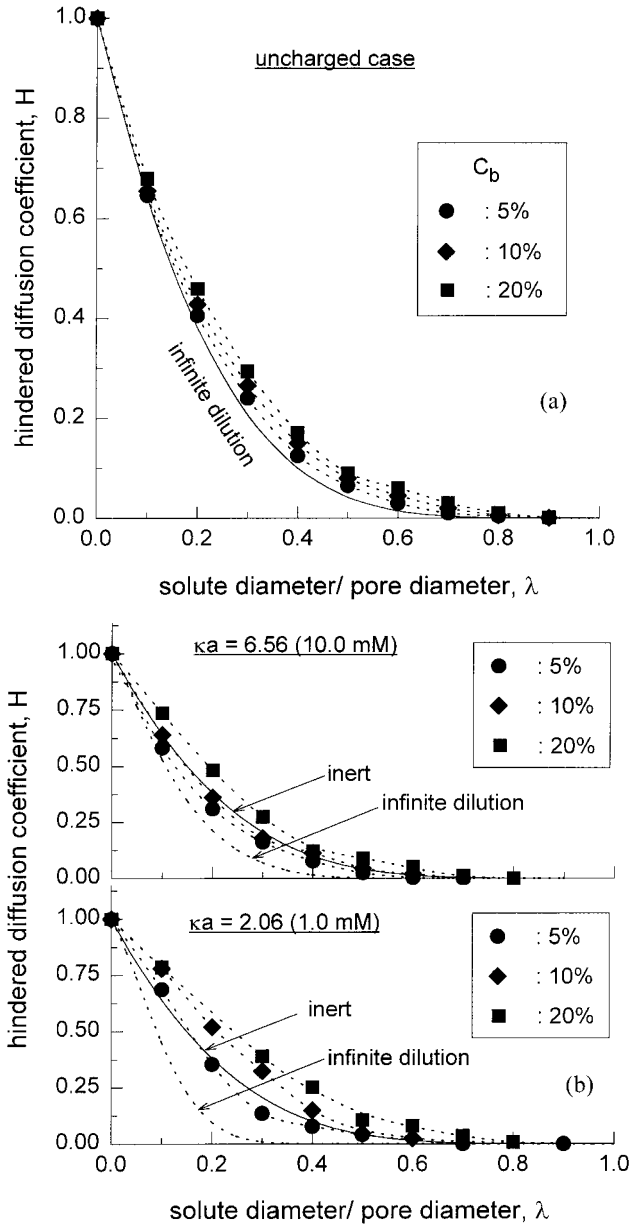

Fig. 9. GEMC results of the hindered diffusion coefficient H at finite bulk concentrations as a function of λ (a) for the purely steric case, (b) for the case of charged wall and charged solutes with solution ionic strengths of 10 and 1 mmol/L

actually in case of highly restricted narrow pores. Slits constrain the solute position only in one dimension, whereas cylindrical pores offer constraints in two dimensions. Accordingly, the wall effects tend to be stronger for cylindrical pores than for slit pores. The behavior of H is similar to K, however, the results for H display certainly a weaker dependence on solute concentration compared to those for K. This is because the contribution of nonhydrodynamic interaction is largely decreased due to the considerable effect of the hydrodynamic coefficient Q^{-1} depending on λ. It is clear that this effect of Q^{-1} is increased with increase of λ. When the solute concentra-

tion increases, both solute-wall and solute-solute interactions must be considered.

Simulation results for ionic strengths of 10 and 1 mmol/L are provided in Fig. 9b. As the thickness of the double layer increases, the importance of the repulsive interactions is enhanced. Due to the contribution of solute-solute and solute-wall repulsive energies, however, the hindered diffusion coefficient can still become greater than in the inert case at concentrations between approximately 5–10%, depending on the ionic strength. At an even larger Debye length, corresponding to $\kappa a = 2{,}06$, the effect of solute concentration is still greater. Compared to the case of $\kappa a = 6.56$, the variations of the H curve become wider with the change of solute concentration.

Conclusions

The partition coefficient is a reflection of the probability of finding the solute within the bulk-like region of the pore, averaged over the pore cross section. Previous results show that the GEMC technique has been proved to be a rigorous scheme to predict the concentration partitioning, compared to the virial expansion and other approximated analytic methods. Therefore, traditional approaches such as the virial expansion method are unable to examine the physicochemical behavior of charged colloidal suspensions with non-dilute solute concentration.

Present simulated results clearly demonstrate that the concentration partitioning can be highly altered by changing the solution environment, in which the partitioning is increased with increasing solute concentration for a given relative pore size. The pairwise additivity principle allows us to estimate the total interaction energy of the system for each random configuration. It has been observed that, when the particle-particle interaction is considered alone with an uncharged pore wall, the partition coefficient for narrow pores is estimated above one, indicating a kind of physical adsorption of solutes onto the pore walls. The influence of solute concentration on the hindered diffusion is not significant in the uncharged case, however, it becomes greater as the solution ionic strength decreases.

Appendix A: Nomenclature

a : solute radius
C : solute concentration
D : diffusion coefficient
D^p : diffusion coefficient in the pore
D_∞ : diffusion coefficient in the bulk
E : interaction energy
e : elementary electrostatic charge
$\boldsymbol{e}$: unit vector
F : electrostatic force
f : Mayer function
H : hindered diffusion coefficient
h : separation distance
$\boldsymbol{I}$: identity tensor
J_s : solute flux
K : partition coefficient
K_t : hydrodynamic function
kT : Boltzmann thermal energy
N : total number of solute particles
$\boldsymbol{n}$: unit normal vector pointing into the solvent
P : pressure
p : governing probability
Q : inverse of enhanced drag
Q_c : convective hindrance factor
Q_d : diffusive hindrance factor
$\boldsymbol{r}, \boldsymbol{r}_1$: position vectors of a sphere
S : surface
T : temperature
$\boldsymbol{T}$: Maxwell stress tensor
V : volume
$\langle v \rangle$: mean velocity
y, z : Cartesian coordinates
β : dimensionless solute position
ε : dielectric constant
η : solvent viscosity
κ : inverse Debye length
λ : ratio of solute diameter to pore diameter
μ : chemical potential
Π : osmotic pressure
σ : dimensionless surface charge density
ψ : electrostatic potential
$\psi_{s,p}$: surface potential of solute particle
$\psi_{s,w}$: surface potential of the wall

Subscripts

r, θ, φ : elements of spherical coordinates

Superscripts

α, β : specified subsystem

Acknowledgement: This work was supported in part by the *Korea Ministry of Science and Technology.* Generous allocations on the Workstation in the *Global Environment Research Center of KIST* are highly acknowledged.

[1] H. Brenner, L. J. Gaydos, *J. Colloid Interface Sci.* **58**, 312 (1977)
[2] D. M. Malone, J. L. Anderson, *Chem. Eng. Sci*. **33**, 1429 (1978)
[3] W. M. Deen, *AIChE J*. **33**, 1409 (1987)
[4] E. D. Glandt, *AIChE J*. **27**, 51 (1981)
[5] J. L. Anderson, J. H. Brannon, *J. Polym. Sci., Polym. Phys. Ed*. **19**, 405 (1981)
[6] B. D. Mitchell, W. M. Deen, *J. Membrane Sci*. **19**, 75 (1984)
[7] F. G. Smith, W. M. Deen, *J. Colloid Interface Sci*. **91**, 571 (1983)
[8] M. G. Davidson, U. W. Suter, W. M. Deen, *Macromolecules* **20**, 1141 (1987)
[9] A. J. Post, *J. Colloid Interface Sci*. **129**, 451 (1989)

[10] N. P. Lin, W. M. Deen, *J. Colloid Interface Sci.* **153**, 483 (1992)
[11] J. M. D. MacElroy, S.-H. Suh, *AIChE Symp. Ser.* **82** (248), 133 (1986)
[12] L. A. Fanti, E. D. Glandt, *AIChE J*. **35**, 1883 (1989)
[13] A. J. Post, D. A. Kofke, *Phys. Rev. A* **45**, 939 (1992)
[14] A. Z. Panagiotopoulos, *Mol. Phys*. **61**, 813 (1987)
[15] A. Z. Panagiotopoulos, N. Quirke, M. Stapleton, D. J. Tildesley, *Mol. Phys*. **63**, 527 (1988)
[16] R. R. Singh, K. S. Pitzer, J. J. de Pablo, J. M. Prausnitz, *J. Chem. Phys*. **92**, 5463 (1990)
[17] D. G. Green, G. Jackson, E. de Miguel, L. F. Rull, *J. Chem. Phys*. **101**, 3190 (1994)
[18] L. F. Rull, G. Jackson, B. Smit, *Mol. Phys*. **85**, 435 (1995)
[19] M.-S. Chun, R. J. Phillips, *AIChE J*. **43**, 1194 (1997)
[20] M. P. Allen, D. J. Tildesley, "*Computer Simulation of Liquids*", Oxford Univ. Press, New York 1987
[21] K. Binder, D. W. Heermann, "*Monte Carlo Simulation in Statistical Physics: An Introduction*", Springer-Verlag, Berlin 1988
[22] W. B. Russel, D. A. Saville, W. R. Schowalter, "*Colloidal Dispersions*", Cambridge Univ. Press, New York 1989
[23] R. J. Phillips, *J. Colloid Interface Sci*. **175**, 386 (1995)
[24] P. M. Bungay, H. Brenner, *Int. J. Multiphase Flow* **1**, 25 (1973)